ISLAMIC UNIVERSITY OF TECHNOLOGY
ORGANIZATION OF THE ISLAMIC CONFERENCE (OIC)

DEPARTMENT OF ELECTRICAL AND ELECTRONIC ENGINEERING

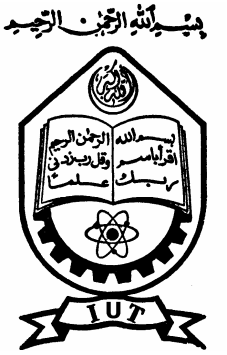

Review of constraining cosmological parameters using 21-cm signal from the era of Reionization.

Supervisor
Mr. Shafiqur Rahman
Assistant professor, EEE, IUT.

Co-supervisor
Mr. Syed Ashraf Uddin Shuvo
Teaching assistant and PhD student
University of Kentucky, USA.

Submitted By
Khan Muhammad (052413)
Md. Emon Hossain Khan (052401)
Ahmed Raihan Abir (052470)

Constraining cosmological parameters using 21-cm signal from the era of Reionization.

This is to certify that the work presented in this thesis is an outcome of the investigation carried out by the authors under the supervision of Mr. Shafiqur Rahman, assistant professor at the Dept. of EEE in Islamic University of Technology (IUT).

Md. Emon Hossain Khan, Author

Supervisor

Mr. Shafiqur Rahman
Assistant professor, Dept. of EEE
Islamic University of Technology

Khan Muhammad Bin Asad, Author

Dr. Md. Shahid Ullah
Head, Dept. of EEE
Islamic University of Techynology

Ahmed Raihan Abir, Author

Abstract

We were very ambitious regarding the outcome of our project. In fact we tried to improvise the necessity of a radio telescope on the far side of the Moon. But later we realized the importance of SKA (Square Kilometer Array) as a feasible tool for unveiling the mystery of the Universe. So we tried to calculate the precise error margins of the cosmological parameters that SKA will give us. As far as we know Fisher4Cast is an efficient tool to constrain the error margins in a astrophysical survey. But we didn't get enough time to use this tool efficiently. So we studied a very important paper by Yi Mao, Max Tegmark et al. to understand the constraints. We learned that, for future experiments, marginalizing over nuisance parameters may provide almost as tight constraints on the cosmology as if 21 cm tomography measured the matter power spectrum directly. Before studying about the constraining process we studied the basic physics of Early Universe, Reionization era, Dark Ages and 21-cm signal. We have written a review on the physics and observational constraints promised by the future telescopes in this thesis report.

Contents

Chapter 1
Introduction

Our main target here is to study the constraining of cosmological parameters by the 21-cm signal. We have presented some data taken from the paper of Mao et al. From these data we have showed that SKA can give better constraints than any other present day telescopes. SKA is the next generation radio telescope.

In the 2nd chapter we revisited the basic Physics of the early universe. We have used a standard textbook and summarized the vital equations and rationales for such realization. In the 3rd chapter we have summarized the Physics of the Dark Ages. Dark ages began after the recombination of almost all the electrons with nucleus. It started 3000 years after the Big Bang and lasted up to the era of Reionization. It's not long that we have come to know an absorption or emission line which indicates a wavelength of 21 cm. From this faint signal many information of the Dark Ages can be extracted. In the 4th chapter we have presented the basic physics of Reionization era as analyzed by the leading cosmologists of this age. Reionization of H in the Intergalactic medium started after the birth of primeval stars and black holes. Specific time of Reionization is yet to be calculated. 5th chapter is on 21 cm cosmology. Here we describe the emission or absorption 21 cm wave. 21-cm cosmology is very important for simulating the intergalactic medium (IGM) during, before of after Reionization.

6th chapter describes the 21cm power spectrum. 7th chapter is on radio interferometers that are operating currently and which are going to start operating soon. Here we have presented the latest specification of SKA which is expected to start operating from 2020. The last that means 8th chapter is on the simulations and results from the paper of Mao, Tegmark et al. From the data we can realize that 21-cm signal will be able constrain the present day cosmology with far more sophistication than CMB. And next generation telescope SKA will be able to observe the 21-cm signal. But for finer observation we have to build a radio telescope on the far side of the Moon.

Chapter 2

Physics of the Early Universe

2.1 Hubble's law

Doppler Effect phenomenon:

The wavelength of light from a moving source increases according to the formula-

$$\lambda' = \lambda(1 + \frac{V}{c})$$

But it has to be modified for relativistic velocities. Considering that the redshift is defined as- $z = \frac{\Delta\lambda}{\lambda}$

Hubble discovered that, $z \propto L$ [Where, L = distance]

Velocity-distance law: $V \approx H \times L$

Where, H = Hubble parameter = 100 $km(\sec^{-1})(Mpec^{-1})$

H is constant throughout the space at a common time but is not constant in time. [1]

2.2 Cosmological principle

Universe is homogenous (all places are alike) and isotropic (all directions are alike). It consists of expanding space. Light from the distant galaxies are redshifted because their separation distance increases due to the expansion of space. Galaxies don't move, empty space between them expands only.

Universe is uniform if it's motion is uniform. Thus there is only dilation (undisturbed expansion). No shear or rotational movements exist. Hubble's law can be easily derived from this cosmological principle.

2.3 Comoving coordinates

Universal scale factor = R(t) ; it's a function of cosmic time, t

R increases in time (but same throughout space) if universe is uniformly expanding or decreases in time if universe is uniformly contracting.

All lengths increase with time in proportion to R, all surfaces in proportion to R^2 and all volumes in proportion to R^3. [1]

If, R_0 = value of scale factor at present time

L_0 = distance between two commoving points, then

Corresponding distance at any other time (t) will be, $L(t) = R(t) \times \frac{L_0}{R_0}$

If an expanding volume V contains N number of particles,

Particle number density, $n = n_0 \times \left(\frac{R}{R_0} \right)^3$

Present average density of matter in the universe = 1 H atom per m^3

At the time at which scale factor was 1% of what it is today average matter density was 1 H atom per cm^3

Velocity-distance law in another form: $V = L \times \frac{\dot{R}}{R}$

where, $\dot{R}$ = rate of increase of scale factor

Unifying two forms of the law we get, $H = \frac{\dot{R}}{R}$

Hubble time or the time of expansion of the Universe, $t_H = H^{-1}$

A rough measure of the age of the Universe, billion years

Where, h = normalized Hubble parameter = between 0.5 and 0.8

Rate of increase of velocity, $\dot{V} = L \times \frac{\ddot{R}}{R}$

Deceleration parameter independent of the particular body at commoving distance L is,

$q \equiv -\frac{\ddot{R}}{RH^2}$

Kinematic classification of the Uniform Universes:

a) (H> 0, q> 0) expanding and decelerating

b) (H> 0, q< 0) expanding and accelerating

c) (H< 0, q> 0) contracting and decelerating

d) (H< 0, q< 0) contracting and accelerating

e) (H> 0, q = 0) expanding with zero deceleration

f) (H< 0, q = 0) contracting with zero deceleration

g) (H =0, q = 0) static.

According to present findings, only a, b and e are the possible candidates for the present state of our Universe. If we extrapolate the expanding scenario backwards, we reach at an extremely high density state when $R \to 0$. Present findings on CMBR suggest, such a state actually existed in the Early Universe and it can be explained by the Big Bang theory.

2.4 Cosmic Microwave Background Radiation (CMBR)

Matter in the early universe should be viewed as a gas of relativistic particles in thermodynamic equilibrium. There was also electromagnetic radiation. Characteristic rate of particle process is in the order of characteristic energy, T.

Rate of the expansion of universe is given by much smaller scale, $H \approx \sqrt{G}T^2 \approx \frac{T}{M_p} \times T$

CMB, once extremely hot, has been cooled over billions of years, redshifted by the expansion of the Universe and has today a temperature of a few degrees Kelvin. Observations from COBE have shown that intensity of CMBR follows the black body curve.

For blackbody radiation, $\lambda_{\max} = \frac{1.26hc}{k_B} \times T$

24-hour anisotropy occurs due to the motion of the galaxy at a speed of 600 km/s. Anisotropy is in the order of only 10^{-5}. They are the imprint of density fluctuations that evolved within the galaxies and clusters.

CMB obeys Planck spectrum which is favorable to expanding universe theory.

Temperature of CMB, $T_{CMB} = 2.725 \pm .002^o K$

2.4.1 Source of CMB

When temperature of the universe was more than 10^{10} K, energy was roughly 1 MeV.

Characteristic energy = $k_B T = m_e c^2$

Particles whose masses were smaller than characteristic energy are: electrons, neutrinos, their antiparticles.

Temperature decreases inversely proportional to the scale factor.

When temperature drops below the characteristic threshold energy, photon can achieve electron-positron pair creation. All electron-positron disappears from plasma, photon decouples and the universe becomes transparent to photon. We detect these redshifted photons as CMB. [2]

2.5 Friedmann Models

It's a solution of General Relativity incorporating cosmological principle: [3]

$ds^2 = dt^2 - R^2(t)d\sigma^2$

$d\sigma^2 = d\chi^2 + f^2(\chi)(d\theta^2 + \sin^2\theta d\phi^2) = d\chi^2 + f^2(\chi)d\Omega^2$

This spatial element describes a three dimensional space with constant curvature.

These are comoving coordinates. So the actual spatial distance between two points (χ, θ, ϕ) and $(\chi_o, \theta_o, \phi_o)$ will be, $d = R(t)(\chi - \chi_o)$

There are three choices for $f(\chi)$:

$$f(\chi) = \begin{cases} \sin\chi (k=1) 0\langle\chi\langle\pi \\ \chi (k=0) 0\langle\chi\langle\infty \\ \sinh\chi (k=-1) 0\langle\chi\langle\infty \end{cases}$$

Here, k = spatial curvature, value of Ricci scalar calculated from $d\sigma^2$ with the scale factor divided out.

k=0: infinite flat space-time with Euclidean spatial geometry

k=1: closed spacetime with spherical spatial geometry

k=-1: open spacetime with hyperbolic spatial geometry

Robertson-Walker metric: $d\sigma^2 = \frac{dr^2}{1-kr^2} + r^2 d\Omega^2$; $r = f(\chi)$

It comes out as a solution of Einstein's equation: $\Re_{\mu\nu} - \frac{1}{2}\Re g_{\mu\nu} - \Lambda g_{\mu\nu} = 8\pi g T_{\mu\nu}$

$\Re = \Re_{\mu\nu} g^{\mu\nu}$; Ricci scalar, $\Re_{\mu\nu}$ = Riemann curvature tensor

$T_{\mu\nu}$ = Matter-energy momentum tensor, G = Newton's constant of Gravitation

Λ = Cosmological constant

In the framework of the Robertson-Walker metric, light emitted from a source at the point χs at time t_S, propagating along a null geodesic $d\sigma^2 = 0$, taken radial $(d\Omega^2 = 0)$ without loss of generality, will reach us at $\chi_0 = 0$ at time t_0 given by, $\int_{t_S}^{t_0} \frac{dt}{R(t)} = \chi s$

Continuity equation expressing the conservation of energy for the comoving volume R^3,

$$\dot{\rho} + 3(\rho + p)\frac{\dot{R}}{R} = 0$$

Friedmann equation determining the evolution of scale factor,

$$\left(\frac{\dot{R}}{R}\right)^2 = \frac{8\pi G}{3}\rho + \frac{\Lambda}{3} - \frac{k}{R^2}$$

Friedmann equation can be written in terms of present Hubble parameter H_0 and present deceleration parameter q_0. Then a critical density is to be defined, $\rho_c = \frac{3H^2}{8\pi G}$

At present time, $\rho_c, 0 = 1.05 \times 10^{-5} h^2 GeVcm^{-3}$

Besides, $\Omega = \frac{\rho_0}{\rho_c}$; then Friedmann equation becomes,

$$\frac{k}{R_0^2} = H_0^2(\Omega_0 - 1 + \frac{\Lambda}{3H_0^2}) \text{ and } q_0 = \frac{1}{2}\Omega_0 - \frac{\Lambda}{3H_0^2}$$

For $\Lambda = 0$ we get, $\frac{k}{R_0^2} = H_0^2(\Omega_0 - 1)$ and $q_0 = \frac{1}{2}\Omega_0$

Therefore, $\begin{cases} \rho_0 \rangle \rho_c, 0 \Rightarrow k = +1 \\ \rho_0 = \rho_c, 0 \Rightarrow k = 0 \\ \rho_0 \langle \rho_c, 0 \Rightarrow k = -1 \end{cases}$

Considering different contribution to the density we can write, [1]

$$\frac{k}{R_0^{\,2}} = H_0^{\,2}(\Omega_m + \Omega_r + \Omega_\Lambda + \Omega_v - 1)$$

2.6 Simple Cosmological Solutions

2.6.1 Empty de Sitter Universe

$p = \rho = 0; k = 0$

So, $H^2 = \frac{\Lambda}{3}$ and $q = -\frac{\Lambda}{3H^2} = -1$

For $\Lambda \rangle 0$ we get, $R(t) = R(t_o) e^{\sqrt{\frac{\Lambda}{3}}(t - t_o)}$

2.6.2 Vacuum energy dominated Universe

Most of energy-momentum tensor comes from vacuum energy.

Here, Energy-Momentum Tensor is, $T_\mu^\nu = -\sigma \delta_\mu^\nu$

Equation of state is, $p = -\rho = -\sigma$ where $\sigma \rangle 0$, is a constant.

Negative pressure of the vacuum can lead to an accelerated exponential expansion.

For $\Lambda = k = 0$, Friedmann-Einstein equation becomes,

$H^2 = \frac{8\pi G}{3}\sigma$ and $q = -\frac{8\pi G \sigma}{3H^2} = -1$

Here scale factor is, $R(t) = R(t_0) e^{(t - t_0)\sqrt{\sigma \frac{8\pi G}{3}}}$

Vacuum dominated universe and empty de sitter universe are physically undistinguishable. [4]

2.6.3 Radiation dominated universe

In the hot and dense early universe there was gas of relativistic particles in thermodynamic equilibrium. There $m << T$ because the particles with $m > T$ are decoupled.

Density of that relativistic gas is, $\rho = \frac{\pi^2}{30} QT^4$

Q = number of degrees of freedom of different particle species

$$= \sum_B g_B + \frac{7}{8} \sum_F g_F$$

g_B and g_F are number of degrees of freedom for each Boson (B) and Fermion (F).

Pressure of relativistic gas, $p = \frac{\pi^2}{90} QT^4 = \frac{1}{3}\rho$

For $\Lambda = k = 0$ Friedmann equation becomes, $H^2 = \frac{8\pi G}{3}\rho = \frac{8\pi^3 Q}{90} T^4$

Radiation term, $\rho \propto R^{-4}$ where R is scale factor. So in the early universe, even if Λ or k are present they are negligible for the scale factor was negligible.

Here, $R(t) = \overline{C}\sqrt{t}, T(t) = \frac{C^{-1}}{\sqrt{t}}, H = \frac{1}{2t}$ where $\overline{C} = (R(t_1)T(t_1))C$, t_1 is any finite time

$$C = \left(\frac{32\pi^3 Q}{90} \right)^{1/4}$$

Deceleration parameter, q = 1

So, radiation dominated universe is under decelerated expansion.

2.6.4 Matter dominated universe

Pressure-less non-relativistic particle's equation of state, $p = 0$

$$\rho(T) = \rho(T_0)\left(\frac{T}{T_0} \right)^3 = \hat{\rho}_0 R^{-3} \text{ where } \hat{\rho}_0 = \rho(T_0) R_0^{\ 3}$$

Einstein-Friedmann equation for $\Lambda = k = 0$ is, $H^2 = \frac{8\pi G\hat{\rho}_0}{3} R^{-3}$

$q = \frac{1}{2}, H = \frac{2}{3t}, R(t) = (6\pi G\hat{\rho}_0)^{1/3} t^{2/3}$

It also undergoes a decelerated expansion.

2.6.5 General equation of state

For deriving equation of state we consider the matter as a fluid rather than gas of particles. And the equation of state becomes, $p = \omega\rho$

Solution of continuity equation with a constant ω, $\rho = \hat{\rho}_0 R^{-3(1+\omega)}$

For expanding universe, $\omega + 1 > 0$

Setting again, $\Lambda = k = 0$ Friedmann equation becomes,

$H^2 = CR^{-3(1+\omega)}, q = \frac{1}{2}(1+3\omega)$

Scale factor, $R(t) = \hat{C}(\omega)(t)^{\frac{2}{3(\omega+1)}}, \hat{C}(\omega) = \left(\frac{3(1+\omega)}{2}\right)^{2/3(\omega+1)} C^{1/3(\omega+1)}$

For an accelerating expansion, $1 + 3\omega < 0 \Rightarrow -1 < \omega < -\frac{1}{3}$

2.7 Effects of curvature and Cosmological constant

Curvature term = $-\frac{k}{R^2}$, becomes important at late times when R is higher.

Radiation term = kR^{-4}, smaller at late times

Matter term = kR^{-3}, smaller at late times

Inserting curvature term in the Friedmann equation for matter dominated universe, [1]

$H^2 = \frac{C}{R^3} - \frac{k}{R^2}$ and $(2q-1)H^2 = \frac{k}{R^2}$ given that $C = \frac{8\pi G\hat{\rho}_0}{3}$

2.7.1 Open, flat space (k=0)

$$R(t)=\left(\frac{9C}{4}\right)^{1/3}t^{2/3}, H=\frac{2}{3t}, q=\frac{1}{2}, \rho=\rho_c=\frac{3H^2}{8\pi G}, \Omega=1$$

2.7.2 Closed, spherical space (k=1)

$R(t)=C\sin^2\varphi(t)$

where $\varphi(t)$ is the solution of $t=C(\varphi-\sin\varphi\cos\varphi)$

Maximal radius of expansion, $R_{\max}=C$, reached at time $\frac{C\pi}{2}$ when Hubble parameter becomes zero. After this time universe will start contracting until R(t) becomes zero at time $C\pi$

$q>\frac{1}{2}, \rho>\rho_c, \Omega>1$

2.7.3 Open, hyperbolic space ($k=-1$)

$R(t)=C\sinh^2\varphi(t)$ Where $\varphi(t)$ is the solution of $t=C(\sinh\varphi\cosh\varphi-\varphi)$

Scale factor increases indefinitely. $\rho<\rho_c, \Omega<1, q<\frac{1}{2}$

2.7.4 Effects of Cosmological constant

Consider a closed k=1 universe with $\Lambda\neq 0$, Friedmann equation will be,

$$H^2=\frac{8\pi G}{3}\rho(R)+\frac{\Lambda}{3}-\frac{1}{R^2}$$

Hubble parameter decreases until it reaches a minimum and then starts increasing again until it reaches an asymptotic value $\Lambda/3$. The scale factor after the Big Bang follows, first radiation dominated and later matter dominated, decelerated expansion, then reaches a

plateau at the value $R_0 = 2\pi G\hat{\rho}_0(1+\sqrt{1+\frac{2\hat{\rho}_1}{3\pi G\hat{\rho}_0{}^2}})$ and finally increases again following an accelerated expansion (Lemaitre Universe).

2.8 Matter density of the Universe

From the previous topic: $H^2 = \frac{8\pi G}{3}\rho(R) + \frac{\Lambda}{3} - \frac{1}{R^2}$

Which can be put into the form, $\frac{k}{R^2} = H^2(\Omega - 1)$

Where, $\Omega = \Omega_m + \Omega_\Lambda$ and $\Omega_\Lambda = \Lambda / 3H^2$

The cosmological constant contribution stands for a general effective vacuum contribution which could have a, for the moment unknown, dynamical origin. For $\Omega > 1$, the Universe is closed and, in the absence of a cosmological constant, the expansion would change into contraction. This is not necessarily true in the presence of a non-zero cosmological constant. In the case $\Omega < 1$ the Universe is open and the expansion continues forever. This is true also for the critical case $\Omega = 1$.

A lower bound for Ω is supplied by the observed Visible Matter $\Omega > 0.03$. Arguments based on Primordial Nucleosynthesis support this value. We can denote $\Omega_{vm} \sim 0.03$. Thus, it seems that most of the mass in the Universe is in an unknown non-baryonic form. This matter is called Dark Matter. In general, such matter can only be observed indirectly through its gravitation. Doing that, one arrives at an estimate $\Omega_{dm} \sim 0.03$.

What is the origin of the remaining contribution to Ω? Since it cannot be attributed to matter, visible or dark, it is represented with an effective vacuum term and has been given the name Dark Energy. For theoretical reasons (i.e. Inflation), the value Ω = 1 is particularly attractive. In that case, the Dark Energy contribution is $\Omega_{de} \sim 0.7$. This estimate is supported by current data[5][6].

Chapter 3

Physics of the Dark Ages

Astronomers have a great advantage. They can see the early universe by telescopes. Light coming from far away is nothing but the image of early universe. But we cannot see the very early or infant universe. Because at that time (up to 400,000 years after BB) universe was opaque due to Thomson scattering. Thus we can only observe the EM waves whose redshift is less than 10^3.

Einstein argued theoretically against cosmological principle. But there is a model in general relativity incorporating cosmological principle. That is Robertson-Walker metric which can be written as:

$$ds^2 = dt^2 - R^2(t)\left[\frac{dr^2}{1-kr^2} + r^2(d\theta^2 + \sin^2\theta d\phi^2)\right]$$

Where, $d\sigma^2 = \frac{dr^2}{1-kr^2} + r^2 d\Omega^2$

Where, $d\Omega^2 = (d\theta^2 + \sin^2\theta d\phi^2)$

R(t) is the scale factor in spherical comoving coordinates (r, θ, φ)

k determines the geometry of the universe.

If distance between two observers is D then on observer will be receding from the other at a velocity H(t)D where H(t) is Hubble parameter at time t.

At constant time t, $H(t) = \frac{dR(t)}{dt}$, $z = \frac{1}{R(t)} - 1$

Friedmann equation can be derived from Einstein field equation.

3.1 Linear gravitational growth

During combination of proton and electron universe was uniform but with small spatial fluctuations in energy density and gravitational potential. It was in the order of only one

part in 10^5. Suppose universe was expanding uniformly. Small perturbations in it can be denoted by,

Density perturbation, $\delta(x) = \frac{\rho(r)}{\overline{\rho}} - 1$

Here the universe has been considered as a pressureless fluid of density ρ

r is the fixed coordinate and x is the commoving coordinate.

Velocity corresponding to the fluid is, $u \equiv v - Hr$

Hubble flow, $v = H(t)r$

Continuity equation in commoving coordinate, $\frac{\partial \delta}{\partial t} + \frac{1}{a}\nabla.[(1+\delta)u] = 0$

Euler equation, [8] $\frac{\partial u}{\partial t} + Hu + \frac{1}{a}(u.\nabla)u = -\frac{1}{a}\nabla\varphi$

Potential φ is given by Poisson equation, $\nabla^2\varphi = 4\pi G\overline{\rho}a^2\delta$

By the above three equations we describe the linear evolution of collision-less cold dark matter particles. It is considered as a fluid. Collisions started after the beginning of non-linearity. Baryons act in the same way when their temperature is low.

For very small perturbations $\delta << 1$ fluid equations can be written as,

$\frac{\partial^2\delta}{\partial t^2} + 2H\frac{\partial\delta}{\partial t} = 4\pi G\overline{\rho}\delta$, this linear equation governs the density evolution which grows by a factor $D(t) \propto \frac{(\Omega_\Lambda a^3 + \Omega_k a + \Omega_m)^{1/2}}{a^{3/2}} \int \frac{a'^{3/2}\, da'}{(\Omega_\Lambda a'^3 + \Omega_k a' + \Omega_m)^{3/2}}$

Spatial form of the initial density fluctuation can be described in Fourier space, [8]

$\delta_k = \int d^3x\delta(x)e^{-i\vec{k}.\vec{x}}$

Magnitude of (commoving wave vector) $\vec{k}$ is k (commoving wave number) which is given by $\frac{2\pi}{\lambda}$

This is very simple for fluctuations generated by inflation. In that case perturbation Is given by Gaussian random field. Statistical properties of the fluctuation are given by the variance of different k-modes statistically independent of each other. The variance is described in terms of power spectrum,

$\langle \delta_k \delta_{k'}^{*} \rangle = (2\pi)^3 P(k) \delta^{(3)}(\vec{k} - \vec{k}')$

Where $\delta^{(3)}$ is the 3D Dirac delta function.

Current inflation models can't give us the overall amplitude of the power spectrum of density fluctuations. It is set by measuring the temperature fluctuation of the observed CMB. Sometimes local measurements are taken.

Details of linear gravitational growth are not being discussed here. Because it is not much relevant to the physics of reionization. Rather we shall directly go to the non-linear growth. It started with the abundance of dark matter halos. Here abundance may refer to the number density of halos as a function of mass. Detail can be found on the paper of Abraham Loeb. [9]

3.2 Post-linear evolution of density fluctuations

3.2.1 Spherical top-hat collapse

Present structures were formed by small density perturbations,

$\delta = \frac{\rho - \bar{\rho}}{\bar{\rho}}$ where ρ is density field

Linear theory of perturbation evolution when $\delta << 1$, $\ddot{\delta} + 2\frac{\dot{a}}{a}\dot{\delta} = 4\pi G \rho \delta$:- Jean's eq.

Initially the perturbed region expands with Hubble flow. But it eventually becomes separated from background universe and collapse.

For a FRW universe equation for top-hat overdensity in SCDM is,

$\ddot{R} = -\frac{4\pi}{3} G \bar{\rho}_m (1 + \delta_m) R$

Virial theorem, $2T + U = 2T + \frac{3}{5} G \frac{M^2}{R} = 0$

Energy conservation between turnaround and virialization, $U_{ta} = U_{vir} + T_{vir} = \frac{1}{2} U_{vir}$

Virial radius, $R_{vir} = \frac{1}{2} R_{ta}$

Density contrast, $\Delta_{vir} = \frac{\rho_m}{\rho_{cr}} \approx 178$

Above equations were for SCDM. Now for ΛCDM and uncoupled DE (dark energy) models, $\ddot{R} = -\frac{4\pi}{3} G[\overline{\rho}_m(1+\delta_m) + \overline{\rho}_{DE}(1+3w_{DE})]R$

Here virial radius, $R_{vir} \neq \frac{1}{2} R_{ta}$

3.2.2 Coupled Dark Energy (cDE) models

Friedmann equation for baryon, radiation, cold DM and DE,

$$\left(\frac{\dot{a}}{a}\right)^2 = \frac{8\pi}{3} G(\rho_r + \rho_b + \rho_c + \rho_{DE}) a^2$$

Continuity equations,

DM-DE interaction is parametrized by, $C = \sqrt{16\pi G/3}\beta$

$$\dot{\rho}_{DE} + 3\frac{\dot{a}}{a}(1+3w_{DE})\rho_{DE} = C\rho_c\dot{\phi} \text{ or } \ddot{\phi} + 2\frac{\dot{a}}{a}\dot{\phi} + a^2 V_{,\phi} = C\rho_c a^2$$

$$\dot{\rho}_c + 3\frac{\dot{a}}{a}\rho_c = -C\rho_c\dot{\phi}$$

$$\dot{\rho}_b + 3\frac{\dot{a}}{a}\rho_b = 0$$

$$\dot{\rho}_r + 4\frac{\dot{a}}{a}\rho_r = 0$$

In this model virialization is defined as,

1 - Only materials within top-hat considered: escaped baryon fraction neglected

2 - All the materials inside the original fluctuation plus intruder DM considered

3.2.3 Spherical collapse model

Spherical collapse model is widely used to understand the formation of early galaxies, that means the formation of non-linear structures. This model can be described by the following points:

1. A single perturbation is considered in a background universe. Both are described by the Friedmann equation. For background universe k=0 and for the perturbation k=+1. Then the equations for the evolution of background universe and perturbed region are formulated. Certain conditions are applied.
2. Density contrast and dimensionless velocity perturbations are formulated. These define the linear regime.
3. It is showed that, the perturbation expands to a maximum or turnaround radius r_{ta}. Overdensity at turnaround radius is formulated.
4. Perturbation collapse to zero radius at $t_c=2t_{ta}$. If there is a slight violation in the exact symmetry of the perturbation than it will not collapse to zero radius. Rather virial equilibrium will be established. That means "Potential energy = -2 × kinetic energy".
5. Post collapse dark matter halo is a singular isothermal sphere for $\Omega_M = 1$

The collapse of a spherical top-hat perturbation is described by the Newtonian equation,

$$\frac{d^2 r}{dt^2} = H_0{}^2 \Omega_\Lambda r - \frac{GM}{r^2}$$

Here, r is the radius of a overdense region in fixed coordinate; H_0 is the present day Hubble parameter; M is the total mass enclosed in the radius r.

Overdensity δ grows initially as, $\delta_L = \delta_i \frac{D(t)}{D(t_i)}$, but eventually it crosses δ_L (Overdensity predicted by linear theory).

Spherical collapse model can explain much of the formation of halos. But the non-linear structure formation in cold dark matter proceeds hierarchically. It is explained in CDM model. Numerical simulation of this hierarchy is presented in the NFW (Navarro, Frenk & White, 1997) model. NFW profile indicates roughly universal spherically-averaged density. NFW profile is,

$$\rho(r) = \frac{3H_0^{\,2}}{8\pi G}(1+z)^3 \frac{\Omega_m}{\Omega_m^z} \frac{\delta_c}{c_N x(1+c_N x)^2} \text{ where, } x = \frac{r}{r_{virial}} \text{ and,}$$

characteristic density, $\delta_c = \frac{\Delta_c}{3} \frac{c_N^{\,3}}{\ln(1+c_N) - \frac{c_N}{1+c_N}}$, c_N = concentration parameter

Most recent N-body simulations are showing deviations from NFW profile. [9]

3.3 Nonlinear growth

An analytic model to match the numerical simulations for measuring number density of halos was developed by Press and Schechter (1974). It is based on: [10]

1. Gaussian random field of density perturbation
2. Linear gravitational growth
3. Spherical collapse

To determine the abundance of halos at a redshift z we use the term δ_M . The probability that δ_M will be greater than a value δ is,

$$\int d\delta_M \frac{1}{\sqrt{2\pi}\sigma(M)} \exp\left(-\frac{\delta^2{}_M}{2\sigma^2(M)}\right) = \frac{1}{2} erfc\left(\frac{\delta}{\sqrt{2}\sigma(M)}\right)$$

Final formula for mass fraction in halos above M at redshift z,

$$F(>M \mid z) = erfc\left(\frac{\delta_{crit}(z)}{\sqrt{2}\sigma(M)}\right)$$

Where $\delta_{crit}(z)$ is the critical density of collapse found for spherical top-hat.

We shall skip the detail equations governing the formation of first stars, supermassive black holes and quasars. Because our target is to understand the physics behind Reionization and the emission of 21-cm H line from IGM. So we will start with radiative feedback from the first sources of light.

Chapter 4

Physics of Reionization

4.1 Radiative feedback from the first sources of light

Intergalactic ionizing radiation field is determined by the amount of ionizing radiation escaped from the host galaxies of stars and quasars. The value of escape fraction is to be determined as a function of redshift and galaxy mass. So far our achievement in determining this is negligible. There are certain problems in understanding the escape route:

- Density of gas within the halo is higher than the IGM
- Halo itself is embedded in an overdense region

So, present day simulations of Reionization era consider the ionizing radiation sources as unresolved point source in the large-scale intergalactic medium. [11]

Escape fraction is very sensitive to the 3D distribution of UV sources relative to the geometry of the absorbing gas within the host galaxy.

Escape ionizing radiation, $h\nu > 13.6eV, \lambda < 912A^0$

Escape fraction from the disks of present-day galaxies has been determined: [12]

Milky Way = 3-14%

Magellanic stream = 6%

Four nearby starburst galaxies = 3%-57%

Current Reionization calculations assume that,

- galaxies are isotropic point sources of ionizing radiation
- escape fraction is in the range of 5-60% [11]

Clumping has a significant effect on the escape of ionizing radiation from inhomogeneous medium. But it introduces some unknown parameters like:

- number of clumps
- overdensity of clumps

- spatial correlation between clumps and ionizing sources
- hydrodynamic feedback from the gas mass expelled from the disk by stellar winds and supernovae

In 2000 Wood and Loeb calculated the escape fraction of ionizing photons from disk galaxies as a function of redshift and galaxy mass. In this calculation escape fractions >10% were achieved for the stars at z~10 only if 90% of the gas was expelled from the disk or if dense clumps removed the gas from the vast majority of the disk volume. [13]

4.2 Propagation of ionization fronts in the IGM

The first stage of this propagation is to produce a H II bubble around each ionizing source which is expanding. When filling factor of these distinct bubbles become significant, they start to overlap thereby beginning the "overlap phase" of Reionization.

H II region is a cloud of glowing gas and plasma, sometimes several hundred light-years across, in which star formation is taking place. Young, hot, blue stars which have formed from the gas emit copious amounts of ultraviolet light, ionizing the nebula surrounding them. H II regions are named for the large amount of ionized atomic hydrogen they contain, referred to as H II by astronomers (H I region being neutral atomic hydrogen, and H_2 being molecular hydrogen). H II regions can be seen out to considerable distances in the universe, and the study of extragalactic H II regions is important in determining the distance and chemical composition of other galaxies.

Assume a spherical ionization volume V separated from the surrounding neutral gas by a sharp ionization front.

- For stars ionization front is thinner
- For quasars ionization front is thicker

In the absence of recombination each H atom in the IGM will only be ionized once. So,

For ionized proper volume, $\overline{n}_H V_p = N_\gamma$

Where, $\overline{n}_H$ = mean number density of H

N_γ = Total number ionizing photons produced by the source

But in case of increased density of the IGM at high redshift recombination cannot be neglected. Balancing recombination and ionization, (for steady ionizing source)

$\alpha_B \bar{n}^2{}_H V_p = \frac{dN_\gamma}{dt}$; α_B = Recombination coefficient (depends on the square of the density)

For non-steady ionizing source, $\bar{n}_H \left(\frac{dV_p}{dt} - 3HV_p \right) = \frac{dN_\gamma}{dt} - \alpha_B \langle n^2{}_H \rangle V_p$ [14]

Recombination depends on the square of the density. If gas in the ionizing source is distributed in high density clumps, then a volume-averaged clumping factor C is introduced where, $C = \langle n_H^2 \rangle \bar{n}_H^2$

If the ionizing source is very large with many clumps, then by unifying above two equations and:

Specifying C and switching to the comoving volume V we get,

$$\frac{dV}{dt} = \frac{1}{\bar{n}_H^0} \frac{dN_\gamma}{dt} - \alpha_B \frac{C}{a^3} \bar{n}_H^0 V$$

Where the present number density of H is, $\bar{n}_H^0 = 1.88 \times 10^{-7} \left(\frac{\Omega_b h^2}{0.022} \right) cm^{-3}$

It is lower than the total number density of baryons $\bar{n}_b^0$ by a factor ~0.76

The solution of V(t) generalized from Shapiro & Giroux (1987),

$V(t) = \int_{t_i}^{t} \frac{1}{\bar{n}_H^0} \frac{dN_\gamma}{dt'} e^{F(t',t)} dt'$ where $F(t',t) = -\alpha_B \bar{n}_H^0 \int_{t'}^{t} \frac{C(t'')}{a^3(t'')} dt''$

Solving it we get, $F(t',t) = -\frac{2}{3} \frac{\alpha_B \bar{n}_H^0}{\sqrt{\Omega_m} H_0} C[f(t') - f(t)] = -.262[f(t') - f(t)]$

Last result is calculated by putting the ideal values of all the parameters. [9]

Here, $f(t) = a(t)^{-3/2}$

For ΛCDM model it can be replaced by, $f(t) = \sqrt{\frac{1}{a^3} + \frac{1 - \Omega_m}{\Omega_m}}$

Average number of ionizations per baryon, $N_{ion} \equiv N_\gamma f_{star} f_{esc}$

N_γ = total number of ionizing photons produced by the source

f_{star} = efficiency of incorporating baryons into stars

f_{esc} = escape frequency

Neglecting recombinations, maximum comoving radius the region which the halo of mass M can ionize is, $r_{\max} = \left(\frac{3}{4\pi}\frac{N_\gamma}{\bar{n}_H^0}\right)^{1/3} = \left(\frac{3}{4\pi}\frac{N_{ion}}{\bar{n}_H^0}\frac{1}{f_{star}}\frac{1}{f_{esc}}\right)^{1/3} = \left(\frac{3}{4\pi}\frac{N_{ion}}{\bar{n}_H^0}\frac{\Omega_b}{\Omega_m}\frac{M}{m_p}\right)^{1/3}$

This actual radius can never be achieved if the recombination time is shorter than the lifetime of the ionizing source. [15]

Production rate of ionizing photons, $\frac{dN_\gamma}{dt} = \frac{\alpha-1}{\alpha}\frac{N_\gamma}{t_s}\times\begin{cases}1; t < t_s\\ \left(\frac{t}{t_s}\right)^{-\alpha} otherwise\end{cases}$

If we consider mini-quasars instead of stars a similar result is obtained. The ionization front around a bright transient source like quasar expands at early times at nearly the speed of light.

General equation for the relativistic expansion of the comoving radius ($r = (1+z)r_p$) of the quasar H II region in an IGM with a neutral filling fraction x_{HI} ,

$$\frac{dr}{dt} = c(1+z)\left[\frac{\dot{N}_\gamma - \alpha_B C x_{HI}(\bar{n}_H^o)^2(1+z)^3\left(\frac{4\pi}{3}r^3\right)}{\dot{N}_\gamma + 4\pi r^2(1+z)cx_{HI}\bar{n}_H^0}\right]$$

c=speed of light, C=clumping factor, α_B = recombination coefficient

$\dot{N}_\gamma$ = rate of ionizing photons crossing a shell at the radius of the H II region at time t.

For $\dot{N}_\gamma \to \infty$ the propagation speed of the proper radius of the H II region r_p approaches the speed of light.

The actual size of the H II region along the line-of-sight to a quasar can be inferred from the extent of the spectral gap between the quasar's rest-frame $Ly\alpha$ wavelength and the

start of $Ly\alpha$ absorption by the IGM in the observed spectrum. These ionized bubbles could be imaged directly by future **21-cm maps** of the regions around the highest-redshift quasars. The profile of the Lyα emission line of galaxies has also been suggested as a probe of the ionization state of the IGM. [9]

4.3 Reionization of Hydrogen

Process of Reionization involves several distinct stages: [11] [9]

1. Pre-overlap stage
2. Overlap stage
3. Post-overlap stage [17]

4.3.1 Pre-overlap

Individual ionizing sources turn on and ionize their surroundings. Galaxies form in the most massive halos and these halos are also formed within the densest regions. Thus ionizing photons escaping from these sources have to pass through a dense region where recombination rate is also big enough to keep H neutral.

When ionizing photons come out of the galaxies and reach IGM, they can propagate more easily through comparatively void medium. Highly ionized regions are separated from neutral regions by ionization fronts. Ionizing intensity is very inhomogeneous. Intensity is determined by distance from the nearest ionizing source and ionizing luminosity of that source.

H II filling factor – the fraction of the volume of the universe which is filled by H II regions. This stage is determined by the evolution of H II filling factor.

Naïve filling factor = F_{HII} =number density of bubbles$\times$average volume of each bubble

Actual filling factor or Porosity = Q_{HII}

General equation for the evolution of H II bubbles, $\frac{dV}{dt} = \frac{1}{\overline{n}_H^0}\frac{dN_\gamma}{dt} - \alpha_B \frac{C}{a^3}\overline{n}_H^0 V$

To meet the transition between the neutral and fully ionized universe we convert this equation to, $\frac{dQ_{HII}}{dt} = \frac{N_{ion}}{0.76}\frac{dF_{col}}{dt} - \alpha_B \frac{C}{a^3}\overline{n}_H^0 Q_{HII}$

F_{col} = collapse fraction, fraction of all the baryons in the universe which are in galaxies

Primordial mass fraction of H = 0.76

4.3.2 Overlap

The central, relatively rapid "overlap" phase of reionization begins when neighboring H II regions begin to overlap. Whenever two ionized bubbles are joined, each point inside their common boundary becomes exposed to ionizing photons from both sources. Therefore, the ionizing intensity inside H II regions rises rapidly, allowing those regions to expand into high-density gas which had previously recombined fast enough to remain neutral when the ionizing intensity had been low. Since each bubble coalescence accelerates the process of reionization, the overlap phase has the character of a phase transition and is expected to occur rapidly, over less than a Hubble time at the overlap redshift. By the end of this stage most regions in the IGM are able to see several un-obscured sources, and therefore the ionizing intensity is much higher than before overlap and it is also much more homogeneous. An additional ingredient in the rapid overlap phase results from the fact that hierarchical structure formation models predict a galaxy formation rate that rises rapidly with time at the relevant redshift range. This process leads to a state in which the low-density IGM has been highly ionized and ionizing radiation reaches everywhere except for gas located inside self-shielded, high- density clouds. This marks the end of the overlap phase, and this important landmark is most often referred to as the "moment of reionization". [9]

4.4 Characteristic Observed Size of Ionized Bubbles at the End of Reionization

Measuring the unknown size distribution of the bubbles at their final overlap phase is a focus of forthcoming observational programs aimed at highly redshifted 21cm emission from atomic hydrogen.

The combined constraints of cosmic variance and causality imply an observed bubble size at the end of the overlap epoch of ~ 10 physical Mpc, and a scatter in the observed redshift of overlap along different lines-of-sight of ~ 0.15. This scatter is consistent with observational constraints from recent spectroscopic data on the farthest known quasars. This result implies that future radio experiments should be tuned to a characteristic angular scale of ~ 0.5 and have a minimum frequency band-width of ~ 8 MHz for an optimal detection of 21cm flux fluctuations near the end of reionization. [16]

From schematic sketch of the thermal history of the Universe we get:
From z~1000 upto z~200 – Both spin and gas temperature track CMB temp. Where $T_\gamma \propto (1+z)$

After z~200 upto z~20 – gas temperature declines as $T_k \propto (1+z)^2$. Spin temp tracks gas temperature through collisional coupling upto a certain level and start declining more slowly than gas temp.
After z~20 – radiations from light sources heat up the kinetic temp. eventually above the CMB temp. Spin temperature tracks CMB temp by radiative coupling.
Finally spin temp once again tracks gas temperature through Wouthuysen-Field effect (The production of a cosmic backgrounds of UV photons between the $Ly\alpha$ and the Lyman-limit frequencies that redshift or cascade into the $Ly\alpha$ resonance).

There are two competing sources for fluctuations in SBO (Surface of bubble overlap) each of which depends on R_{SBO}, ionized region just before the final overlap:

1. 21cm signals observed from different points along the curved boundary of H II region must have been emitted at different times.

2. Bubbles on a comoving scale R achieve reionization over a spread of redshifts due to cosmic variance in the initial conditions of the density field smoothed on that scale.

Let, physical radius of a H II region = $\frac{R}{1+\langle z\rangle}$

For a 21cm photon, light crossing time of this radius is, $\langle \Delta z^2 \rangle^{1/2} = \left|\frac{dz}{dt}\right|_{\langle z\rangle} \frac{R}{c(1+\langle z\rangle)}$

For high redshifts, $\frac{dz}{dt} = -H_0 \sqrt{\Omega_m}(1+z)^{5/2}$

Collapsed fraction, $F_{col}(M_{\min}) = erfc\left[\frac{\delta_c - \bar{\delta}_R}{\sqrt{2[\sigma_{R_{\min}}{}^2 - \sigma_R^2]}}\right]$

$$\Rightarrow \frac{\delta z}{1+z} = \frac{\bar{\delta}_R}{\delta_c(\bar{z})} - \left[1 - \sqrt{1 - \frac{\sigma_R^2}{\sigma_{R_{\min}}^2}}\right]$$

$\delta_z =$ offset between the redshift when a region of mean overdensity $\bar{\delta}_R$ achieves this critical collapsed fraction, and the redshift $\bar{z}$ when the Universe achieves the same collapsed fraction on average.

$\delta_c(\bar{z}) =$ collapse threshold $\propto (1+\bar{z})$

4.5 Reionization era can give important information about Early Universe

After the Big Bang, the Universe was a hot, but quickly cooling soup of fundamental particles. After a few hundred thousand years, things cooled enough so that protons and electrons could combine to form neutral hydrogen. This was a rather sudden event, and allowed the thermal glow of the fireball plasma, as it existed immediately before the hydrogen formation event, to radiate throughout the universe unimpeded by constant interactions with the charged particles of the now-absent plasma. This glow, redshifted by a factor of 1100 or so is what we now observe as the Cosmic Microwave Background (CMB) in all directions. The CMB carries a frozen imprint of the density fluctuations in

the early Universe, the study of which, by the observational cosmology community, is intense and sustained.

During recombination at z=1100, universe was almost uniform with small density perturbations in the order of 10^{-5}. These small perturbations increased with time and eventually caused spherical collapse. Before spherical collapse, evolution of the universe can be explained by linear theories of Physics and Mathematics. But with top-hat spherical collapse non-linear evolution of the density perturbations started.

- Linear evolution of density perturbations is explained by the ΛCDM model. It actually denotes the evolution of cold dark matter halos.
- Non-linear growth started when cold dark matter halos became abundant. This evolution can be explained by cDE and Spherical collapse models.

Small substructures started to form with spherical collapse. Photo-reionization of the neutral H could not be possible if first luminous sources didn't formed. This reionization was caused by the UV rays from population III stars and x-rays from the black holes. But stars and black holes cannot be formed without the formation of galaxies. Now, astronomers think that, dwarf galaxies started to form when the universe was 100 million years old. These dwarf galaxies created big galaxies by merging together. Reionization started with the emission of EM waves from the stars, quasars and black holes and their escape from the galaxies. These escaped radiations created ionized bubbles in the IGM. These bubbles grew up and overlapped to fill the entire IGM with ionized H.

Reionization era was the transition between the dark ages and the formation of stars and massive galaxies. So, By studying reionization, we can learn a great deal about the process of structure formation in the universe, and find the evolutionary links between the remarkably smooth matter distribution at early times revealed by CMB studies, and the highly structured universe of galaxies and clusters of galaxies at redshifts of 6 and below. Following points can be considered as the principal causes of studying Reionization:

1. Properties of the intergalactic medium or IGM. At present IGM is filled with gases in the plasma state. But it contradicts the early recombination process. We identified these plasma state gases by the anisotropies of CMB. But details on the formation and evolution of these IGM matters can be explained by studying the epoch of reionization.

2. Once the first sources produce photons capable of ionizing the surrounding IGM, the process of reionization (and reheating) can be thought of having begun, thus changing the thermal, ionization and chemical properties of the IGM. This change in the nature of the IGM affects the formation of next generation of sources (like metal enrichment changing the initial mass function of stars). So we can reveal the secrets of forming varieties of enriched structures in the universe by studying reionization.

3. First two points are associated with IGM and it's feedback in forming the later structures. The next important feature of reionization study is the formation of dwarf galaxies. Reionization suppressed the formation of low-mass galaxies. UV rays from these dwarf galaxies reionized the neutral H of IGM, but eventually this ionized H suppressed the formation of it's creator. It occurred due to the heating of cosmic gas up to a certain level. [18]

4. Altogether, the critical parameter for any source considered for ionizing IGM can be summarized as its "emission rate of hydrogen-ionizing photons per unit cosmological volume." With these constraints, it is expected that quasars and first generation stars were the main sources of energy of the Reionization. Quasars do not exist in high enough numbers to reionize the IGM alone, saying that "only if the ionizing background is dominated by low-luminosity AGNs can the quasar luminosity function provide enough ionizing photons." So we can learn much about Quasars and AGNs by studying reionization.
5. Hot, large, Population III stars which will form supernova are a possible mechanism for reionization. Population III stars are currently considered the most

likely energy source to initiate the reionization of the universe. Because unlike population II stars they radiate much photons to ionize H. We have not been able to detect these stars so far. So simulations of cosmic reionization are a great way to learn about these stars, their formation and how they contributed in the evolution of early universe.

Chapter 5

21-cm Cosmology

The dark ages even have one key advantage over the CMB: because the IGM is no longer affected by photon diffusion, the baryons develop fluctuations on scales down to the Jeans mass in the neutral IGM. In principle, this permits tests of the matter power spectrum on much smaller scales than the CMB does.

A particularly fascinating set of questions relate to the epoch of reionization, the hallmark event of the high-redshift Universe. It is the point at which structure formation directly affected every baryon in the IGM, even though only a small fraction of them actually resided in galaxies. It also marked an important phase transition for galaxies: once the IGM was ionized, it became transparent to ultraviolet (UV) photons – a dawn (of sorts) for the young galaxies inhabiting the high-redshift Universe.

5.1 Fundamental physics of 21cm line

5.1.1 Brightness temperature

Fundamental quantity = Brightness or Specific Intensity (I_υ)

= ray emerging from a cloud at frequency υ

= energy carried by rays traveling along a given direction per unit area, frequency, solid angle and time. So unit is "ergs s^{-1} cm^{-2} sr^{-1} Hz^{-1}"

Angle averaged specific intensity, $J_\nu = \int I_\nu d\Omega$

I_ν is quantified by equivalent brightness temperature $T_b(\nu)$. $I_\nu = B_\nu(T_b)$

B_ν = spectrum of equivalent blackbody radiation [24]

$T_b(\nu) \approx \frac{I_\nu c^2}{2k_B \nu^2}$ (Rayleigh-Jeans formula – excellent approximation to Planck carve for 21cm line, acquired from Planck's radiation law)

Rest frequency of 21cm line = 1420.4057 MHz

$$T_b(\nu) = \frac{T_b^{'}(\nu)}{1+z}$$

$T_b'(\nu) =$ Emergent brightness temperature of a cloud measured in its comoving frame

$T_b(\nu) =$ Apparent brightness of that cloud at Earth

Observed frequency, $\nu = \frac{\nu_0}{1+z}$

5.1.2 Flux density

Flux produced by an individual gas cloud at Earth, $S = \int_{cloud} I_\nu \cos\theta d\Omega d\nu$

Frequency dependent incident energy flux = S_ν (unit is Jansky)

$$S_\nu = I_\nu \Delta\Omega = \frac{2k_B T_b \nu^2 \Delta\Omega}{c^2}$$

$T_b'(\nu) = T_{ex}(1-e^{-\tau_\nu}) + T_R'(\nu)e^{-\tau_\nu}$ - most important equation

Here, $T_{ex} =$ uniform excitation temperature of cloud

$T_R' =$ Brightness temperature of CMBR

$\tau_\nu =$ Optical depth = $\int ds\alpha_\nu$

s = proper distance

$\alpha_\nu =$ Absorption co-efficient

5.1.3 Spin temperature

For 21cm radiation $T_{ex} = T_S =$ spin temperature $= \frac{n_1}{n_0} = \frac{g_1}{g_0} e^{-E_{10}/k_B T_S}$

$$= 3e^{-T_*/T_S}$$

Where, $T_* = \frac{E_{10}}{k_B} = 0.68 =$ equivalent temperature

$E_{10} =$ Energy splitting between hyperfine levels 1 and 0.

As $T_S >> T_*$, every 3 of 4 atoms are in the excited state. So, α_ν must have a correction factor for stimulated emission.

Here only one spin temp has been assigned for the entire Hydrogen distribution which is not necessarily correct. *Boltzmann equation* is to be solved in this case as it couples spin temperature and velocity distribution. [25]

When collision time is long coupling between spin temp and velocity distribution introduces percent level changes in brightness temperature.

5.1.4 Optical depth

Optical depth of a cloud of Hydrogen,

$$\tau_\nu = \int ds \sigma_{01} (1 - e^{-E_{10}/k_B T_S}) \phi(\nu) n_0 \approx \sigma_{01} \left(\frac{h\nu}{k_B T_S} \right) \left(\frac{N_{HI}}{4} \right) \phi(\nu)$$

$$\sigma_{10} = \frac{3c^2 A_{10}}{8\pi \nu^2}$$

A_{10} = Spontaneous emission coefficient of the 21cm line

After much refining the final equation of optical depth of 21cm line is,

$$\tau_\nu = \frac{3}{32\pi} \frac{hc^3 A_{10}}{k_B T_S \nu_0^2} \frac{x_{HI} n_H}{(1+z) \frac{dv_{II}}{dr_{II}}} \approx 0.0092 (1+\delta)(1+z)^{3/2} \frac{x_{HI}}{T_S} \left[\frac{H(z)/(1+z)}{\frac{dv_{II}}{dr_{II}}} \right]$$

$(1+\delta)$ = Fractional overdensity of baryons.

$\frac{dv_{II}}{dr_{II}}$ = Gradient of the proper velocity along the line of sight.

There are two main uses of the equation no. 10:

1. Contrast between high-redshift Hydrogen cloud and CMB
2. Absorption against high-redshift radio sources.

5.1.5 Contrast between high-redshift Hydrogen cloud and CMB

$$\delta T_b(\nu) = \frac{T_S - T_\gamma(z)}{1+z}(1 - e^{\tau_{\nu_0}}) = \frac{T_S - T_\gamma(z)}{1+z}\tau_{\nu_0}$$

From above equations we can get the final equation,

$$\delta T_b(\nu) = 9 x_{HI}(1+\delta)(1+z)^{1/2}\left[1 - \frac{T_\gamma(z)}{T_S}\right]\left[\frac{H(z)/(1+z)}{dv_{II}/dr_{II}}\right] mK$$

$T_S >> T_\gamma$ – then δT_b saturates and positive

$T_S << T_\gamma$ – then δT_b is negative and maybe very large.

So observability of 21cm line depends on mainly spin temperature. It's value with respect to CMB temperature defines whether 21cm signal will be detected as emission or absorption line or not at all.

$$T_S^{-1} = \frac{T_\gamma^{-1} + x_c T_K^{-1} + x_\alpha T_C^{-1}}{1 + x_c + x_\alpha}$$

Here, x_c and x_α are coupling coefficients.

5.2 Temperatures of Dark ages

5.2.1 Three temperatures

21-cm electromagnetic radiation or photons emit from neutral H by a process called spin-flipping. Spin-flipping needs much less energy than the energy needed for the electrons to jump to a higher orbit. CMBR energy and energy from the collisions of atoms can provide this much energy, stars or black holes are not needed. So 21-cm photons were produced before the formation of stars that means in the dark ages. We can study dark ages by this 21-cm photon. [21]

- Spin temperature - measure of relative abundance of atoms with aligned spins.
- Kinetic temperature - measure of the motion of the atoms
- Radiation temperature - measure of the energy of the CMB photons

5.2.2 Ménage a trois

Three competing processes determine spin temperature:

1. Absorption and stimulated emission of CMB photons
2. Collisions with other H atoms, free electrons and protons
3. Scattering of UV photons

These processes give rise to three different stages:

- Spin temp matched kinetic temp - 10 million years after BB CMB became too dilute to supply enough energy to the residual free electrons, gas started to cool rapidly. Neutral H was a net absorber of 21-cm photon.
- Spin temp matched radiation temp - 100 million years after BB collision among atoms became too infrequent. Spins picked up energy from CMB. When equilibrium established H atom was neither a net absorber nor a net emitter of 21-cm photon. Gas could not be seen against CMB.
- Spin temp matched kinetic temp - Started after the formation of stars and black holes. X-ray and UV-ray were absorbed and reradiated from H atoms. Spin temp increased beyond radiation temperature, so H outshone the CMB. Galaxies caused the H to glow well before they reionized it. [22]

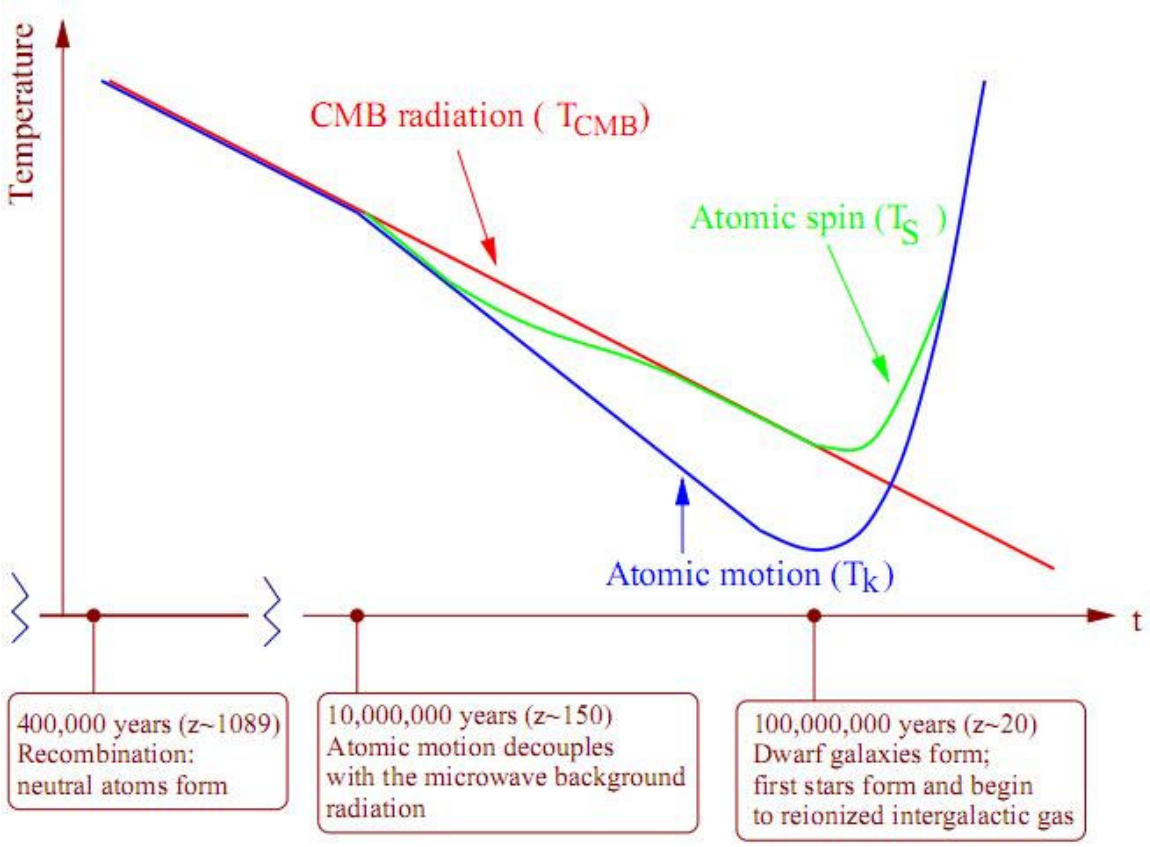

Figure 1: In the above diagram a graphical representation can be seen. From this diagram a detail picture of the three temperatures of the Dark Ages have been realized. [26]

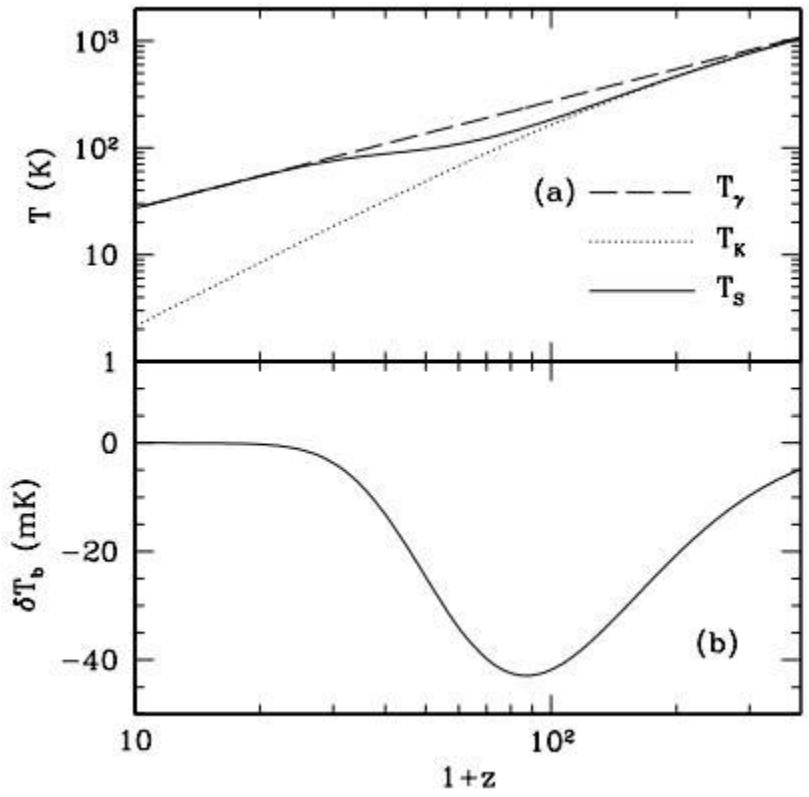

Figure 2: IGM temperature evolution if only adiabatic cooling and Compton heating are involved. The spin temperature T_s includes only collisional coupling. (b): Differential brightness temperature against the CMB for T_s shown in panel a. [27]

5.3 Global history of IGM

δT_b = 21cm brightness temperature with respect to CMB

$\overline{\delta T_b}$ = Globally averaged δT_b

To understand the reionization history we have to compute the evolution of $\overline{\delta T_b}$. This calculation has to be done in some representative structure formation model.

5.3.1 Five critical points in 21cm history

01. z_{dec} - Compton heating becomes inefficient and for the first time $T_K < T_\gamma$

The scattering of photons by stationary free electrons results in energy transfer from the photons to the electrons due to the recoil effect (*Compton heating*). Conversely, the scattering of soft photons by high energy electrons results in a transfer of energy from the electrons to the photons (*Compton cooling*). Thus, Compton scattering can act as a source of heating or cooling so as to bring the plasma into thermal equilibrium with the radiation field.

This is the earliest epoch when 21cm line can be observed.

Thermal decoupling occurs when $1+z_{dec}=150\left(\frac{\Omega_b h^2}{0.023}\right)^{2/5}$

Compton heating becomes inefficient when z~300 and negligible when z~150.

After this point it obeys the equation of adiabatically expanding non-relativistic gas-

$T_K \propto (1+z)^2$

Dark ages begin with this stage. This is the starting critical transition in the IGM history observation with 21cm signal.

02. Density falls below δ_{coll}. $T_S \to T_\gamma$. No 21cm line.

At the beginning of this stage,

x_α = Wouthuysen field coupling coefficient = 0

At sufficiently high redshifts neutral atoms were colliding resulting in collisional coupling.

x_c = Collisional coupling coefficient = 1 when density is δ_{coll}

δ_{coll} = Critical overdensity of collisional coupling.

$$1+\delta_{coll}=1.06\left[\frac{\kappa_{10}(88K)}{\kappa_{10}(T_S)}\right]\left(\frac{0.023}{\Omega_b h^2}\right)\left(\frac{70}{1+z}\right)^2$$

By z~30 IGM essentially becomes invisible.

03. z_h - IGM is heated above CMB temp.

04. z_c - $x_\alpha = 1$, so $T_S \to T_K$

05. z_r - Reionization

Last three stages are visible through luminous objects. But their sequence is source-dependent. For example-

- Pop II stars - z_c precedes z_h. A significant absorption epoch may provide information on first sources.
- Very massive Pop III stars – similar N_α (no. of eV photons per stellar baryon)
- An early mini-quasar population – no absorption epoch.

Advantages of 21cm tomography

- Probing the majority of the cosmic gas, instead of the trace amount (~ 10^{-5}) of neutral hydrogen probed by the Lyα forest after reionization.
- 21cm signal is simply shaped by gravity, adiabatic cosmic expansion, and well-known atomic physics, and is not contaminated by complex astrophysical processes that affect the intergalactic medium at z < 30.
- By 21cm measurements we can know exactly when and how reionization occurred.
- 21cm fluctuations can distinguish between,
    - Fast, late vs. extended, complex reionization
    - Inside-out vs. outside-in reionization
- It can probe first luminous sources.
- Potential to revolutionize our understanding of the epoch of reionization.
- It is more significant than CMB because,
    - CMB map is 2D, and it's 3D
    - CMB only gives information about matters that worked as the seeds of galaxy. But 21-cm photons not only give information about seeds of galaxy but also inform us about the effect of already formed galaxies on it's surroundings.

Chapter 6

21-cm Power Spectrum

Our main task in observing 21-cm signal is to calculate the change in brightness temperature. We usually determine how much this temperature is fluctuating over time, actually over redshift. Power spectrum is a key factor in this regard. For 21-cm the definition of power spectrum can be written as, "power spectrum P(k) is the three-dimensional Fourier transform of the corresponding two-point function and thus parameterizes the correlations present in the appropriate field." [27]

In 5.4 we have discussed the fractional perturbation to the brightness temperature which is denoted by δ_{21}. From the equation of this perturbation we can visualize the power spectrum step-by-step.

6.1 Fractional perturbation to the brightness temperature

Equation for fractional perturbation to the brightness temperature of 21cm signal is,

$$\delta_{21}(x) \equiv \frac{\delta T_b(x) - \delta\overline{T_b}}{\delta\overline{T_b}}$$

It's Fourier Transform is of interest to us,

$$\langle \tilde{\delta}_{21}(k_1)\tilde{\delta}_{21}(k_2)\rangle \equiv (2\pi)^3 \delta_D(k_1+k_2)P_{21}(k_1)$$

Brightness temperature depends on a number of parameters. These can be shown by an equation of the perturbation,

$$\delta_{21} = \beta\delta_b + \beta_x\delta_x + \beta_\alpha\delta_\alpha + \beta_T\delta_T - \delta_{\partial\nu}$$

Here, each δ_i represents fractional variation in a particular quantity. Their definitions are:

δ_b = perturbation term for baryonic density

δ_α = for Lyman alpha coupling coefficient, x_α

δ_x = for neutral fraction. If you use ionized fraction than sign will be changed

δ_T = for kinetic temperature, T_K

$\delta_{\partial v}$ = LOS peculiar velocity gradient.

Here, β_i are the expansion coefficients. And also $T_C = T_K$, where T_C is the color temperature of the Lyman-alpha background.

In this equation everything is isotropic except the LOS peculiar velocity gradient. So we can get two kind of fluctuations in 21-cm signal.

6.2 Fluctuations in 21cm signal

6.2.1 Isotropic fluctuations

All of the four fluctuations below are expected to be statistically isotropic because the physical processes responsible for them do not have any preferred direction-

1. Fluctuations in density
2. Fluctuations in ionization fraction
3. Fluctuations in Lyman-α flux.
4. Fluctuations in temperature.

For these fluctuations, $\delta(\bar{k}) = \delta(k)$. But this assumption may break down in extremely large scales. [28]

6.2.2 Anisotropy in 21cm signal

Two effects break down the isotropy of 21cm signal and create certain anisotropies-

1. Peculiar velocity- the velocities which cannot be explained by Hubble's law-gradients introduce redshift space distortions. For this velocity a gradient is introduced.
2. Transverse and LOS distances scale differently in non-Euclidean space-time which artificially distorts the appearance of any isotropic distribution.

Effects which cause anisotropy are AP effect and redshift-space distortions. These effects are described in 6.3 and 6.4.

6.3 Power spectrum of 21cm fluctuations

Once T_s grew larger than T_γ the gas appeared in 21cm emission. The ionized bubbles imprinted a knee in the power spectrum of 21cm fluctuations, which traced the H I topology until the process of reionization was completed. 21cm fluctuations can probe astrophysical (radiative) sources associated with the first galaxies, while at the same time separately probing the physical (inflationary) initial conditions of the Universe. In order to affect this separation most easily, it is necessary to measure the three-dimensional power spectrum of 21cm fluctuations.

21-cm signal measures the baryon density of the universe directly. Here baryon density δ_b is written as only δ. From 6.1 we know that,

$\langle \tilde{\delta}_{21}(k_1)\tilde{\delta}_{21}(k_2)\rangle \equiv (2\pi)^3 \delta_D(k_1+k_2)P_{21}(k_1)$

Here P_{21} is power spectrum. Basic form of power spectrum is $P_{\delta_i\delta_j}$. We can take any density parameters to calculate power spectrum for those particular parameters. So, for fractional perturbation to neutral fraction we can write δ_x here.

Power spectrum can be of two types:

- Three dimensional Fourier transform of corresponding 2-point function which is called 3D power spectrum.
- Angular power spectrum.

For 21-cm signal we only use the 3D power spectrum. Angular one is preferred for CMB. Angular one is not used in 21-cm cosmology because on large scales the angular fluctuations don't trace corresponding density fluctuations. [27]

Now we can write the final equations for power spectrum. In this case,

Ionization power spectrum, $P_{xx} = \bar{x}_i^2 P_{\delta_x\delta_x}$

Density-ionization power spectrum, $P_{x\delta} = \bar{x}_i P_{\delta_x\delta}$

Total 21-cm power spectrum can be written as three terms with different angular dependence,

$$P_{\Delta T}(k) = P_{\mu^0}(k) + P_{\mu^2}(k)\mu^2 + P_{\mu^4}(k)\mu^4$$

Where, $P_{\mu^0} = P_{\delta\delta} - 2P_{x\delta} + P_{xx}$

$$P_{\mu^2} = 2(P_{\delta\delta} - P_{x\delta})$$

$$P_{\mu^4} = P_{\delta\delta}$$

6.4 Redshift space distortions

In cosmology, third dimension is not radial distance but redshift which are related by the Hubble expansion law but also affected by peculiar velocities. Mainly two effects are responsible for redshift space distortions-

On small scales, particles with same distance can have different redshift because of random motion within e.g. clusters of galaxies. This elongates structures along the line of sight. Apparent clustering amplitude is reduced due to this elongation in redshift space created by random motions in virialized regions. This is called *Fingers of God Effect*. It can be summarized like this- Structures have a tendency to point toward the observer.

On the other hand on very large scales the opposite happens. Objects fall in towards overdense regions. This makes objects between us and the overdensity appear to be further away and objects on the other side of the overdensity appear closer. The net effect is to enhance the overdensity rather than smear it out. These effects are known as *Kaiser Effect*. In this case, the signal is compressed by the infall onto massive structures and apparent clustering amplitude is enhanced. [29]

These anisotropies allow us to separate the astrophysical and cosmological contributions to the 21cm fluctuations.[30] After considering anisotropies, brightness temperature fluctuations in Fourier space has the form,

$\tilde{\delta}_{21} = \mu^2 f\tilde{\delta} + \tilde{\delta}_{iso}$ [28]

Here, μ = cosine of the angle between wave vector **k** and LOS direction

$$f = d\ln\frac{D}{d\ln a} \approx \Omega_m^{0.6}(z)$$ [F-293]

$\tilde{\delta}_{iso}$ can be obtained from the equation.

Neglecting second order terms and setting f=1 for higher redshifts the final equation of power spectrum can be written as,

$$P_{21}(\bar{k}) = \mu^4 P_{\delta\delta} + 2\mu^2 P_{\delta_{iso}\delta} + P_{\delta_{iso}\delta_{iso}}$$

Because of the simple form of this polynomial, measuring the power at ≥ 3 values of μ will allow us to determine $P_{\delta\delta}, P_{\delta_{iso}\delta}, P_{\delta_{iso}\delta_{iso}}$ for each k. Later we can isolate the contribution from density fluctuation $P_{\delta\delta}$.

6.5 Alcock-Paczynski Effect

Previously we have considered that the underlying cosmological model is already accurately known by means of CMB and other signatures. But in reality, using an incorrect cosmological model creates apparent errors in the scaling of angular sizes which depends on, D_A =angular diameter distance. This error is understood by comparing with line of sight sizes which depends only on Hubble parameter. This error introduces artificial anisotropies even in an intrinsically isotropic distribution. This is called Alcock-Paczynski (AP) Effect. AP effect can be used to calculate cosmological parameters though it's quite tough.

Distortions in Ly-α forest can be used to measure AP effect, but there are substantial problems. 21cm signal will be much more useful and efficient to give precise measurements of AP effect for the following reasons,

1. 21ccm signal is all-sky so does not depend on galaxy clusters or Quasar positions.
2. It does not suffer from sparseness problem. [31]

To keep pace with the previous discussion we have to present AP effect in the form of power spectrum. AP effect distorts the shape and normalization of 21cm power spectrum to:

$$P_{21}(k) = \mu^6 P_{\mu^6}(k) + \mu^4 P_{\mu^4}(k) + \mu^2 P_{\mu^2}(k) + P_{\mu^0}(k)$$

Here, 4, 2 and 0 powers of μ are nothing new because they were present in the AP less equation of power spectrum. But P_{μ^6} term is new and hence results solely for AP effect. It therefore allows a measurement of,

$$(1+\alpha) = \frac{HD_A(assumed - \cos mo \log y)}{HD_A(true - \cos mo \log y)}$$

From this equation we can measure H, Hubble parameter. So far, we have got three parameters, baryon density δ_b, Ω_m and H.

From existing cosmological models we have already measured the value of H which will be taken as assumed cosmology. This cosmology is based on CMB observations. But as we can see, through 21cm signal AP effect can be measured more precisely and thus H can be optimized. Here, we constrain cosmological parameters by varying them until α becomes 0.

Universe is very close to Einstein-de Sitter universe at high redshifts. In this kind of flat universe the equation of angular diameter distance is,

$$D_A(a) = a\int_a^1 \frac{da'}{a'^2 H(a')}$$

From this equation it can be realized that AP effect remains sensitive to background cosmology out to high redshifts. [32]

6.5.1 Separating out the AP Effect on 21cm fluctuations

R. Barkana's paper on this topic sheds some light on the massive advantages of 21cm signal over other signatures for constraining cosmological parameters. He started the abstract with the line, "*We reconsider the Alcock-Paczynski effect on 21cm fluctuations from high redshift, focusing on the 21cm power spectrum.*"

He formulated the following results in this paper:

1. At each accessible redshift both the angular diameter distance (D_A) and the Hubble constant (H) can be determined from the power spectrum.
2. This is possible using anisotropies that depend only on linear density perturbations and not on astrophysical sources of 21cm fluctuations.

Measuring these quantities at high redshift would not just confirm results from the cosmic microwave background but provide appreciable additional sensitivity to cosmological parameters and dark energy.

Chapter 7

Interferometer arrays and sensitivity

In this section our main target is to accumulate the formulas required to calculate the sensitivity of an interferometer to the 3D 21cm power spectrum. It should be noted that we are not dealing with angular power spectrum for the reason discussed in the previous chapter. Morales calculated the angular dependence of 3D 21cm signal and McQuinn et. al. extended those in their 2005 paper. [33]

7.1 Interferometric visibility

21cm signal will be observed by arrays of radio telescope antennas or interferometers. Interferometers measure the visibility or fringe amplitude which in this case is quantified as temperature. First, we are considering a pair of antennae.

Visibility, $V(u,v,\nu) = \int d\hat{n}\Delta T_b(\hat{n},\nu)A_\nu(\hat{n})e^{2\pi i(u,v).\hat{n}}$

Here, u,v – number of wavelengths between the antennae

$A_\nu(\hat{n})$ - Contribution to the primary beam in the direction n

Universe is flat that means Einstein-de Sitter

We assume, visibilities are Gaussian random variables

For n visibilities, Covariance matrix, $C_{ij} = \langle V_i^* V_j \rangle$

Likelihood function can be thought as a reversed version of conditional probability. In conditional probability we find out unknown outcomes based on known parameters. But in Likelihood function we find out unknown parameters based on known outcomes. In this case, we know the outcomes according to the cosmological models but confused about parameters.

Here, Likelihood function, $L(\overline{C}) = \frac{1}{\pi^n \det \overline{C}} \exp(-\sum_{i,j}^{n} V_i^* C_{ij}^{-1} V_j)$ [33]

7.2 Detector noise

For receiving the signal through interferometer we use a RMS Detector. It gives a DC voltage output which is determined by the logarithmic level of an AC input. For upcoming arrays covariance matrix **C** will be dominated by detector noise mostly. [33] So it is a key aspect in improving sensitivity.

RMS Detector noise fluctuation per visibility of an antennae pair after observing for a time t_o in one frequency is, $\Delta V^N = \frac{\lambda^2 T_{sys}}{A_e \sqrt{\Delta \nu t_0}}$

Where, $T_{sys}(\nu) =$ total system temperature

$A_e =$ Effective area of an antenna

$\Delta\nu =$ Width of the frequency channel

If we Fourier transform the observed visibilities in the frequency direction then we will have a 3D map of intensity as a function of **u** that means in **u**-space.

$$I(\bar{u}) = \int d\nu V(u,v,\nu) e^{2\pi i \nu \eta}$$

If we perform this transform for only detector noise component than after subsequent calculations we will get the equation of Detector noise covariance matrix,

$$C_{lb}^N(\bar{u}_i, \bar{u}_j) = \left(\frac{\lambda^2 B T_{sys}}{A_e} \right) \frac{\delta_{ij}}{B t_0} \quad [33]$$

In this equation there is no $\Delta\nu$ term, so it only depends on B. Here finer frequency resolution comes with no additional cost. But in case of angular power spectrum, both B and $\Delta\nu$ terms are present in the equation of covariance matrix. [34] Again 3D power spectrum is giving us some advantages.

7.3 Average observing time

We have discussed μ and it's various degrees in chapter three. Here,

$\mu = \bar{k}.\hat{n}$ where **k** is the Fourier dual of the comoving position vector **r**.

Actually **k** is nothing but the wave vector whose value is the wave number k and direction is nothing but the direction of propagation of the wave. It is way of expressing

both the wavelength and direction of the wave. Wave number is nothing but the wavelength.

Now we have to transfer everything from u to k ergo the equation will be expressed in k-space instead of u-v plane. Relationship between u and k,

$$\bar{u}_{\perp} = d_A \bar{k}_{\perp} [\mathrm{Y}]$$

Average observing time for an array of antennae to observe a mode k as a function of total observing time t_0 is expressed as $t_{\bar{k}}$.

$$t_{\bar{k}} \approx \frac{A_e t_0}{\lambda^2} n[\frac{x|\bar{k}|\sin\theta}{2\pi}]$$

7.4 Angular averaged sensitivity

According to the expression of average observing time previous equation of covariance matrix has to be changed for k-space. The equation will be,

$$C^N(\bar{k}_i, \bar{k}_j) = \left(\frac{\lambda^2 B T_{sys}}{A_e}\right)\frac{\delta_{ij}}{Bt_k}$$

After subsequent simplifications McQuinn et. al. paper deduced the following equation for covariance matrix where there are certain contributions of sample variance,

$$C^{SV}(\bar{k}_i, \bar{k}_j) \approx P_{\Delta T}^{21}(\bar{k}_i)\frac{\lambda^2 B^2}{A_e x^2 y}\delta_{ij}$$

The error can be calculated from these equations. Error in the 3D power spectrum of 21cm signal, $P_{\Delta T}^{21}(\bar{k}_i)$ can be expressed as,

$$\delta P_{\Delta T}^{21}(k,\theta) \approx \sqrt{\frac{1}{N_c}}\frac{A_e x^2 y}{\lambda^2 B^2}\left[C^{SV}(k,\theta) + C^N(k,\theta)\right]$$

Error in $P_{\Delta T}^{21}(\bar{k}_i)$ from a measurement in an annulus with $N_c(k,\theta)$ pixels can be measured from the above equation. This error calculation is mandatory for sensitivity measurements.

Spherically averaged signal can be obtained by summing up all pixels in a shell with same wave number. After measuring all pixels in shell with constant k, the equation of error will be,

$$\delta P_{\Delta T}(k) = \left\{ \sum_{\theta} \left[\frac{1}{\delta P_{\Delta T}(k,\theta)} \right]^2 \right\}^{-1/2}$$

Finally, $$\delta P_{\Delta T}(k) \approx \left(k^3 \int_{\arccos\{\min[\, yk/2\pi \,],1\}}^{\arcsin\{\min[(k^*/k),1]\}} d\theta \sin\theta \frac{1}{\left\{ DP_{21}(k) + \frac{E}{[n(k\sin\theta)]} \right\}^2} \right)^{-1/2}$$

Where, k* - longest wave vector perpendicular to LOS probed by the array.
LOFAR will be able to observe N separate view of fields simultaneously. In this case we have to divide the final equation by $N^{1/2}$.

7.5 Foreground

Aside from the problems of extracting 21cm signal due to terrestrial interference and other Earth related problems, there is a huge backdrop in this field of Radio Astronomy research. That is the problem of foreground. 21cm signal is coming from a very high redshift and passes many regions of high brightness temperature before reaching us. It can be said that, we want to analyze the background, but foreground is disturbing us. The brightness temperature of these foregrounds is sometimes 10,000 times higher than that of 21cm signal. So it's very hard to extract the pure 21cm signal. But in this paper we will only discuss the Interferometer sensitivities. Terms relating to foreground will be omitted.

7.6 Sensitivity of future Interferometers

Currently three massive projects to study the radio universe is going on namely MWA (Australia), LOFAR (Netherlands) and SKA. They all are in different stages of planning and design. MWA and LOFAR are already in implementation stage, but the site of SKA has not yet been decided. For statistical observation MWA is better than LOFAR. [33] But SKA surpasses all of them, it can be called the new generation radio telescope array.

Success of LOFAR and MWA will affect the implementation of SKA largely. SKA may start operating from 2020. Many researchers around the globe have proposed various specifications for it. Specifications mentioned by A. R. Taylor in his paper to the International Astronomical Union is presented on Appendix A.

Chapter 8
Constraining Cosmological Parameters

Calculations have shown that Square Kilometer Array (SKA) will be able to sensitively probe comoving megaparsec scales which are essentially smaller than scales observed by galaxy surveys and comparable to the scales observed with Lyα forest. [33] In CMB constraints of cosmological parameters there are certain degeneracies which can be broken by this new 21cm observation.

21cm signal is most sensitive to cosmological parameters when density fluctuations dominate over spin temperature and neutral fraction fluctuations. McQuinn and others examined this era in their 2005 paper. The reason that neutral hydrogen allows mapping in three rather than two dimensions is that the redshift of the 21 cm line provides the radial coordinate along the line-of-sight (LOS). [35]

There are three position-dependent quantities that imprint signatures on the 21 cm signal:

1. hydrogen density
2. neutral fraction
3. spin temperature

For cosmological parameter measurements, only the first quantity is of interest, and the last two are nuisances. (For some astronomical questions, the situation is reversed.) The 21 cm spin-flip transition of neutral hydrogen can be observed in the form of either an absorption line or an emission line against the CMB blackbody spectrum, depending on whether the spin temperature is lower or higher than the CMB temperature.

8.1 Reference experiment for simulation

Yi Mao has calculated the almost exact constraints on cosmological parameters that SKA will give us compared to other telescopes. He has used Fisher matrix to calculate many parameters and their error margins. Using Lambda-CDM model he has simulated for 4

different telescope settings. Then he has compared those results. I have checked his results and found that SKA is the best solution in our hand for the sake of time. We haven't considered the FFTT. We looked upon all data presented in the paper. [35] But as this is not our original work we are presenting a selected set of data to show that SKA is the best available solution to us. We are starting with the configuration of interferometers.

The planned configuration of the interferometers are quite varied. However, all involve some combination of the following elements, which we will explore in our calculations:

1. A nucleus of radius R_0 within which the area coverage fraction is close to 100%.
2. A core extending from radius R_0 our to R_{in} where there coverage density drops like some power law r^{-n}.
3. An annulus extending from R_{in} to R_{out} where the coverage density is low but rather uniform.

First we are presenting the specifications for Lambda-CDM model. Yi Mao has simulated for 3 different models: Optimistic, pessimistic and medium. We are presenting only the OPT one. Detail can be found on the main paper.

8.2 Lambda-CDM model

The term 'concordance model' is used in cosmology to indicate the currently accepted and most commonly used cosmological model. Currently, the concordance model is the Lambda CDM model. In this model

- The Universe is 13.7 billion years old
- It is made up of
    - 4% baryonic matter
    - 23% dark matter
    - 73% dark energy

The Hubble constant for this model is 71 km/s/Mpc. The density of the Universe is very close to the critical value for re-collapse. Detail specifications are attached at the appendices.

8.3 Optimistic reference model

Various assumptions are made while simulating. Based on the assumptions model can be labeled as,

- Optimistic (OPT)
- Middle (MID)
- Pessimistic (PESS)

Here we have used the optimnistic model. Assumptions in optimistic (OPT) model,

- Abrupt reionization at z<7
- Redshift range = 6 – 10
- Observation time = 16000 hours continuously
- Collecting area = double of design values
- Non-linear cutoff scale k-max is 4 per megaparsec

8.4 Simulation

From the reference paper we are presenting data for the variation of only 4 parameters:

- Redshift ranges
- Array layout
- Collecting area
- Observation time and system temperature

8.4.1 Varying redshift ranges

The results show that, from 21cm data alone, the constraints from the extreme ranges differ significantly (a factor of 5 for ΔΩ_k). Therefore, the sensitivity of a 21cm telescope depends strongly on the frequency range over which it can observe the signal.

Telescopes	z-range	$\Delta\Omega_\Lambda$	$\Delta \ln \Omega_m h^2$	$\Delta \ln \Omega_b h^2$	Δn_s	$\Delta \ln A_s$	$\Delta\Omega_k$
SKA	6.8-10	.0032	.031	.061	.0058	.12	.012
	6.8-8.2	.0038	.044	.083	.0079	.16	.023
	7.3-8.2	.0053	.059	.11	.011	.21	.042
LOFAR	6.8-10	.021	.20	.34	.049	.67	.086

Table 4: How cosmological constraints depend on the redshift range in OPT model. Same assumptions as in Table V but for different redshift ranges and assume only OPT model.

8.4.2 Varying array layout

Furlanetto investigated how array layout affects the sensitivity to cosmological parameters.

Experiment	R_0 (m)	R_{in} (m)	η	n	Comments
SKA	211	1.56	.09	.83	Quasi-giant core
LOFAR	319	1.28	.71	6	Almost a giant core

Table 5: Optimal configuration for various 21cm interferometer arrays. Same assumptions as in previous table but for different array layout. η is the ratio of the number of antennae in the nucleus to the total number inside the core. n is the fall-off index.

8.4.3 Varying collecting area

Survey volume and noise per pixel is affected by collecting area. But it has been shown that varying collecting area does not significantly affect parameter constraints.

Telescopes	$A_e / A_e^{fiducial}$	$\Delta\Omega_\Lambda$	$\Delta \ln \Omega_m h^2$	$\Delta \ln \Omega_b h^2$	Δn_s	$\Delta \ln A_s$
SKA	2	.0027	.048	.099	.0077	.19
	1	.0038	.044	.083	.0079	.16
	0.5	.0043	.043	.076	.0089	.15
LOFAR	1	.025	.27	.44	.063	.89

Table 6: How cosmological constraints depend on collecting areas in the OPT model. Same assumptions as in previous tables but for different collecting areas A_e and assume only OPT model.

8.4.4 Varying observation time and system temperature

The detector noise is affected by changing the observation time and system temperature. We know that, noise,

$$P^N \propto \frac{T_{sys}}{t_0^2}$$

Where T_{sys} is the system temperature and t_0 is the observation time.

Therefore, for noise dominated experiments,

$$\frac{\delta P_{\Delta T}}{P_{\Delta T}} \propto \frac{1}{\sqrt{N_c}} \propto \frac{T_{sys}^2}{t_0}$$

Detector noise is affected by observation time and system temperature. So sensitivity is affected and thus is affected the constraints on cosmological parameters. Order unity changes in these two parameters can change the accuracy of cosmological parameters significantly.

Telescopes	t_0	$\Delta\Omega_\Lambda$	$\Delta \ln \Omega_m h^2$	$\Delta \ln \Omega_b h^2$	Δn_s	$\Delta \ln A_s$
SKA	4	.0089	.0035	.0056	.0065	.022
	1	.014	.0049	.0081	.012	.037
	0.25	.023	.0090	.015	.031	.075
LOFAR	1	.13	.083	.15	.36	.80

Table 7: How constraints on cosmological parameters depend on observation time.

Chapter 9
Conclusion

From the simulations done by Yi Mao it has been realized that SKA will be able to constrain cosmological parameters more precisely than any other radio interferometers of the present day. So it is a feasible project. Over the years the specifications of SKA will be revised more precisely and the best model will be implemented. It has been shown that SKA can really lead the way of new generation radio telescopes.

Also, it has been realized that 21cm signal is far more effective than CMB. Because, CMB map is 2D, and it's 3D. CMB only gives information about matters that worked as the seeds of galaxy. But 21-cm photons not only give information about seeds of galaxy but also inform us about the effect of already formed galaxies on it's surroundings.

But there are certain difficulties in observing 21cm signal. Such as, Ionospheric opacity, Ionospheric phase errors and Terrestrial Radio Frequency Interference (RFI). Best available way to solve these problems is constructing a 21-cm observatory on the far side of the moon. The reason is that, the far side of the moon is an attractive site for setting up a RT primarily because it is always facing away from the earth and is thus completely free from radio frequency interference from transmitters either on earth or in orbit around the earth. After the success of SKA this option can be considered seriously.

Appendices

Appendix A

Parameter	**Specification**
Frequency range	70 MHz – 25 GHz
Sensitivity	$\frac{A_{eff}}{T_{sys}} = 5{,}000$ - 10,000 depending on frequency
Field of view (FOV)	200 to 1 deg^2 depending on frequency
Angular resolution	0.1 arcsecond – 1.4 GHz
Instantaneous bandwidth	25% of band center, maximum 4 GHz
Calibrated polarization purity	10,000:1
Imaging dynamic range	1,000,000:1 at 1.4 GHz
Output data rate	1 Terabyte per minute

Table: SKA specifications by A. R. Taylor.

Appendix B

Name of the parameters	**SKA specifications**
No. of antennas, N_{ant}	7000
Minimum base line	10 m
Field of view, FOV	$\pi 8.6^2 \deg^2$
Effective are, A_e at redshift, z = 6 z = 8 z = 12	 30 50 104
Angular resolution	0.1 second (at z~7)
System temperature, T_{sys} at z = 8 z = 10	 440 K 690 K

Table: SKA specifications used in simulation by Yi Mao et al.

Appendix C

Parameters	**Standard value**
Spatial curvature, Ω_k	0
Dark energy density, Ω_Λ	0.7
Baryon density, Ω_b	0.046
Hubble parameter, h	0.7
Reionization optical depth, τ	0.1
Massive neutrino density, Ω_υ	0.0175
Scalar spectral index, n_s	0.95
Scalar fluctuation amplitude, A_s	0.83
Tensor-to-scalar ratio, r	0
Running of spectral index, α	0
Tensor spectral index, n_t	0
Dark energy equation of state, w	-1

Table: Cosmological parameters in Lambda-CDM model.

References

[1] Kyriakos Tamvakis, An Introduction to the Physics of the Early Universe, University of Ioannina, Greece.

[2] A. A. Penzias and R. W. Wilson, Ap. J. 142, 419 (1965).

[3] A. Friedmann, Zeitschrift fur Physik, 10, 377 (1922) and 21, 326 (1924). Both translated in Cosmological Constants, edited by J. Bernstein and G. Feinberg, Columbia Univ. Press (1986).

[4] A. H. Guth, Phys. Rev. D23, 347 (1981).

[5] A. G. Riess et al., PASP, 116, 1009 (1998); S. Perlmutter et al., Ap. J. 517, 565, (1999).

[6] D. N. Spergel et al., Ap. J. Suppl. , 148, 175 (2003).

[7] P. J. E. Peebles: The Large-Scale Structure of the Universe (Princeton: PUP) (1980)

[8] E.W. Kolb, & M. S. Turner: The Early Universe (Redwood City, CA: Addison-Wesley) (1990)

[9] Abraham Loeb, First Light; astro-ph 0603360.

[10] W. H. Press, & P. Schechter: ApJ 193, 437 (1974)

[11] N. Y. Gnedin: ApJ 535, 530 (2000)

[12] J. B. Dove, J. M. Shull, & A. Ferrara: (1999) (astro-ph/9903331)

[13] K. Wood, & A. Loeb: ApJ 545, 86 (2000)

[14] P. R. Shapiro, & M. L. Giroux: ApJ 321, L107 (1987)

[15] J. Scalo: ASP conference series Vol 142, The Stellar Initial Mass Function, eds. G. Gilmore & D. Howell, p. 201 (San Francisco: ASP) (1998)

[16] J. S. B. Wyithe & A. Loeb: Nature 432, 194 (2004)

[17] T. Roy Choudhury, A. Ferrara; Physics of Cosmic Reionization; astro-ph 0603149

[18] Effect of Cosmic Reionization on the substructure problem in Galactic halo - H. Susa, M. Umemura; 2008.

[19] M. Zaldarriaga, S. R. Furlanetto & L. Hernquist: ApJ 608, 622 (2004)

[20] R. Barkana, & A. Loeb: ApJ, 609, 474 (2004)

[21] G. B. Field: Proc. IRE, 46, 240 (1958); G. B. Field: Astrophys. J. 129, 536 (1959); G. B. Field: ApJ 129, 551 (1959)

[22] Abraham Loeb & Matias Zaldarriaga; Measuring the Small-Scale Power Spectrum of Cosmic Density Fluctuations through 21 cm Tomography Prior to the Epoch of Structure Formation. Physical Review Letters, Vol. 92, No. 21, Paper No. 211301; May 25, 2004.

[23] D. Scott, & M. J. Rees: MNRAS 247, 510 (1990)

[24] John D. Kraus; Radio Astronomy, 2nd edition. Ohio State University.

[25] C. M. Hirata, K. Sigurdson, submitted to Mon. Not. R. Astron. Soc. (astro-ph/0605071).

[26] Yi Mao; Constraining cosmological and gravitational parameters using Astrophysical data. MIT, June 2008.

[27] Steven R. Furlanetto , S. Peng Oh , and Frank H. Briggs; Cosmology at Low Frequencies: The 21 cm Transition and the High-Redshift Universe. September 2006.

[28] M. McQuinn, O. Zahn, M. Zaldarriaga, L. Hernquist, S. R. Furlanetto, submitted to Astrophys. J. (astro-ph/0512263).

[29] S. R. Furlanetto, Mon. Not. R. Astron. Soc. 371 (2006) 867–878.

[30] R. Barkana, A. Loeb, Astrophys. J. 624 (2005) L65–L68.

[31] A. Nusser, Mon. Not. R. Astron. Soc. 364 (2005) 743–750.

[32] S. S. Ali, S. Bharadwaj, B. Pandey, Mon. Not. R. Astron. Soc. 363 (2005) 251–258.

[33] Judd D. Bowman, Miguel F. Morales, Jacqueline N. Hewitt; Constraints on fundamental cosmological parameters with upcoming redshifted 21cm observations. February, 2008.

[34] Wilkinson Microwave Anisotropy Probe (WMAP) Three Year Results: Implications for Cosmology. Authors: D. N. Spergel, R. Bean, O. Doré, M. R. Nolta, C. L. Bennett, J. Dunkley, G. Hinshaw, N. Jarosik, E. Komatsu, L. Page, H. V. Peiris, L. Verde, M. Halpern, R. S. Hill, A. Kogut, M. Limon, S. S. Meyer, N. Odegard, G. S. Tucker, J. L. Weiland, E. Wollack, E. L. Wright.

[35] Yi Mao, Max Tegmark, Matthew McQuinn, Matias Zaldarriaga, and Oliver Zahn; How accurately can 21 cm tomography constrain cosmology?; July 2008.